

Study of surface cleaning before passivation and rear boron doping on high efficiency PERL solar cells

WENJIA LI^a, ZHENJIAO WANG^b, PEIYU HAN, YONGQIAN WANG^c, ZHENGRONG SHI^{c,d}, GUOHUA LI^{a,d,*}

^aJiangnan University, Wuxi 214122, China

^bKingstone Semiconductor Co., Ltd, Shanghai 201203, China

^cSuntech Power Co., Ltd, Wuxi 214028, China

^dJiangsu (Suntech) Institute for Photovoltaic Technology, Wuxi 214028, China

Two cleaning methods (SC-1,2 and SPM) before passivation and four boron sources (two kinds of spin-on boron dopant and two types of PECVD-deposited boron dopant) and three kinds of rear PECVD-deposited boron dopant layers (abbreviated as SiO₂(B), SiN_x(B) and a-Si(B)) are investigated. SPM was selected as the cost-effective cleaning method. PECVD-deposited p-type layer doped by diborane (B₂H₆) was chosen. SiO₂(B) layers with different thicknesses were investigated and 100nm is suitable. Moreover, SiN_x(B) layers with different refractive indices were studied and 2.1 is better. Finally, firing conditions were discussed for cells with a-Si(B). 19.8% efficiency was achieved with 400°C, 1100mm/min firing.

(Received February 9, 2015; accepted April 5, 2016)

Keywords: PERL solar cells, Surface cleaning, Boron source, Boron dopant layer

1. Introduction

Passivated emitter and rear-locally diffused (PERL) solar cell, which benefits from low rear surface recombination (SRV) and locally boron-doped back surface field (BSF), presented high efficiency [1-2]. Many dielectric layers, such as SiO₂/SiN_x stack, Al₂O₃/SiN_x stack and amorphous silicon (a-Si)/SiN_x stack were synthesized to reduce SRV [3-6].

Before passivation, a non-contaminated surface must be created by cleaning for achieving high open-circuit voltages (V_{oc}) [7], because the surface and interface recombination will be amplified in subsequent metallization processes and result in a very low V_{oc} and shunt resistance (R_{sh}) [8]. Therefore, purity of wafer surface is an essential factor for successful fabrication of high efficient silicon solar cells. RCA cleaning was firstly investigated by Kern and Puotinen in 1965. Murarkal et al. [9] concluded that RCA cleaning before oxidation is an effective way for oxidizing Si without introducing stacking faults. Cacciato et al. [10] proposed that SPM-like cleaning is a useful step to guarantee a stable Al₂O₃-based passivation process.

Dating back to 1970s, laser doping started to be employed in semiconductor fabrication [11]. The doping source can be gas, liquid or solid. Samples can be immersed in gases (such as PH₃ [12] or PCl₃ [13]) and organic solutions [14]. Alternatively, dopant layers may be evaporated [15], sputtered [16] or spun [17-19] on wafers prior to laser doping process. Z. Hameiri [17] claimed that Spin on Dopant (SOD) source seemed to be the preferred option. In order to create a solid dopant source, however, the film must be solidified by a short bake after spinning. In addition, the wafers have to experience a HF dip after

laser doping to remove the dopant layer. The concentration of HF solution and the duration of HF immersion should be strictly and precisely controlled to thoroughly clean the wafer and not to destroy the SiN_x layer on both sides. Moreover, the wafers have to undergo a N₂ drying before rear metallization. The increase of production steps (such as bake, removal of SOD layer and N₂ drying) is one of the main reasons of the delay in the industrialization of PERL solar cells.

Moreover, boron-doped PERL cells cannot tolerate a high firing temperature in order to form the boron back surface field [20]. However, low temperature firing could not provide enough energy to gasify the organic impurities in silicon induced by liquid boron source during laser doping, which impeded the improvement of efficiency. Therefore spinning should be replaced by some other methods and boron dopant layer formed by Plasma Enhanced Chemical Vapor Deposition (PECVD) is investigated in this paper. Gall et al. [21-22] reported that if SiN_x is directly deposited on lightly doped Si substrate, the surface passivation performance would be negatively affected by the presence of boron because of a high D_{it} level of SiN_x(B) layer [23]. Thus in order to promote the rear passivation effect, a thin Al₂O₃ film was inserted between silicon bulk and SiN_x(B) [24].

This paper focuses on the tradeoff between the increase of production steps and the cost-effectiveness for PERL cells. In particular (1) two kinds of RCA-like cleaning methods (SC-1,2 (standard cleaning solution 1 and 2) and SPM) before passivation were discussed; (2) the doping profiles of doping sources-Al, B40, PBF1, B₂H₆ and trimethyl boron (TMB) were quantified and the best one was selected; (3) the boron dopant layer SiO₂(B), SiN_x(B) or a-Si(B) was fabricated subsequent to the

passivation layer (SiN_x) by PECVD. As a result, a-Si(B) was selected as the most appropriate boron dopant layer. Since passivation layer and boron dopant layer were both formed by PECVD, the two processes can be integrated into one process and simplify the fabrication process.

2. Experimental

PERL cells were fabricated on $125\text{mm} \times 125\text{mm}$, $200\mu\text{m}$ -thick, $1-3\Omega\text{cm}$, p-type Cz mono-crystalline silicon wafers by following steps: alkaline texturing, acid single-side polishing, thermal emitter diffusion ($55\Omega/\square$) and wet-edge isolation (WEI). Three groups of samples with different sheet resistances were prepared by changing the WEI parameter. After WEI, two cleaning strategies were carried out: 1) aqueous ammonia (NH_4OH)-hydrogen peroxide (H_2O_2) mixture (SC-1) and then hydrochloric acid (HCl)- H_2O_2 mixture (SC-2); 2) sulfuric acid (H_2SO_4)- H_2O_2 mixture (SPM). The flow diagram of SC-1,2 and SPM is showed in Fig. 1. Subsequent to cleaning, SiO_2 (prepared by thermal oxidation) and SiN_x (deposited via microwave remote PECVD) stacks were fabricated. The thickness of SiO_2 on both sides is 10nm and the thicknesses of SiN_x are 80nm (front side) and 200nm (rear side). After passivation, boron dopant layer was deposited by 13.56MHz radio frequency (RF) PECVD. The boron source is B_2H_6 or TMB, while the source dopant layer is $\text{SiO}_2(\text{B})$, $\text{SiN}_x(\text{B})$ or a-Si(B). For p-type layer $\text{SiO}_2(\text{B})$, four different thicknesses were studied. They are 600nm (group A), 400nm (group B), 200nm (group C) and 100nm (group D), respectively. For $\text{SiN}_x(\text{B})$ layer, two kinds of refractive indices (2.1 and 2.3) were investigated. Then, laser (355nm , Coherent) ablation and doping with pitch and width of lines of 1mm and $18\mu\text{m}$ was conducted. Rear aluminum was deposited by physical vapor deposition (PVD) after laser ablation and doping. A standard co-firing step in a belt furnace was performed. The best firing condition for cells with 100nm a-Si(B) p-type layer was decided through experiment. Light induced plating (Ni/Cu/Ag) was employed for the front metallization. The whole flow diagram is demonstrated in Fig. 2.

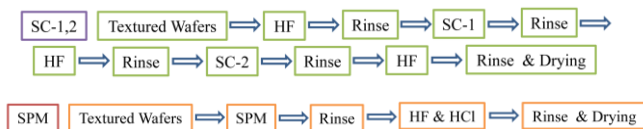


Fig. 1. Flow diagram of SC-1,2 and SPM

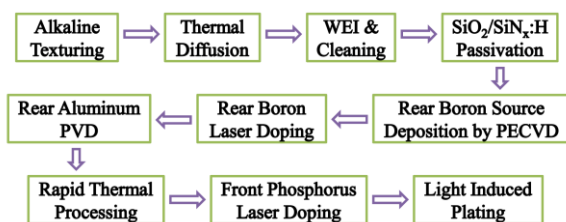


Fig. 2. Flow diagram of fabrication

Effect of SC-1,2 and SPM solutions on surface topography was estimated by analyzing reflectivity of wafers after cleaning. In order to evaluate the influence of cleaning solutions on cells' stability and repeatability, sheet resistances were respectively measured subsequent to WEI, cleaning and thermal oxidation by Semi-lab 2000. Furthermore minority carrier lifetime and implied V_{oc} were measured by quasi-steady-state photo-conductance (QSSPC) techniques after passivation. Alternatively, doping profiles of doping sources (B_2H_6 , TMB, PBF1, B40 and Al) were evaluated by Electro Chemical Voltage (ECV) measurement using a NH_4F electrolyte and a ring surface of 0.101cm^2 . The electrical performance was measured under standard illumination conditions ($\text{AM } 1.5\text{G}$, 1000 W/m^2 , 25°C).

3. Results and discussion

3.1 Satisfied passivation with effective cleaning method

Reflectivity of wafers after SC-1,2 and SPM cleaning are presented in Fig. 3. The reflectivity of wafers cleaned by different methods show a similar trend from 320nm to 1100nm , which indicates that the optical property of wafers does not show obvious difference. Therefore it is concluded that the surface morphology is rarely affected by SC-1,2 cleaning although SC-1 contains alkaline solution (NH_4OH) which can corrode the silicon surface.

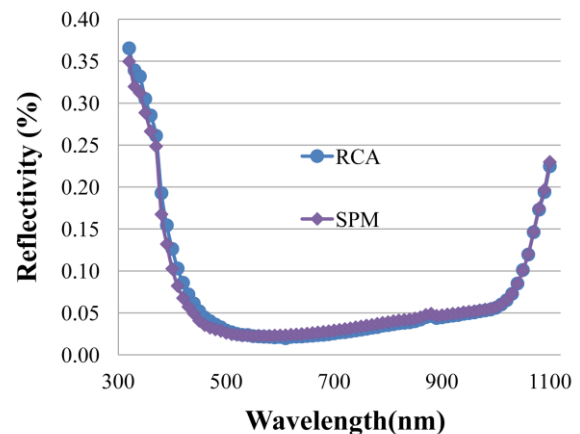


Fig. 3. Reflectivity of wafers cleaned by SC-1,2 and SPM

Fig. 4 demonstrates four groups of sheet resistances which were collected after WEI (i), cleaning (ii) and thermal oxidation (iii) respectively. As shown in Fig. 4, the higher the sheet resistances after WEI are, the less the sheet resistances increase. However, this increase is nonlinear: the growth of groups A, B, C and D from step (i) to step (ii) are $15\Omega/\square$, $14\Omega/\square$, $9\Omega/\square$ and $7\Omega/\square$, while the rise from step (ii) to step (iii) are $23\Omega/\square$, $21\Omega/\square$, $18\Omega/\square$ and $13\Omega/\square$, respectively. This phenomenon is caused by nonlinear and time-varying exothermic chemical reactions

of SC-1,2 solution [25-26]. It is essential, but also very difficult, to provide an accurate control of temperature and PH value of SC-1,2 solutions for a stable cleaning performance considering the nonlinear and time-varying characteristic. By contrast, SPM cleaning does not bring such a variation of sheet resistance as SPM solutions do not contain alkaline solution which can etch the wafers. In this case, SPM cleaning is superior to SC-1,2 cleaning.

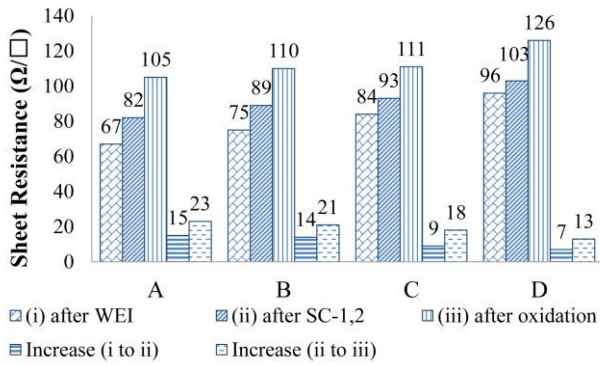


Fig. 4. Sheet resistance after WEI (i), cleaning (ii) and thermal oxidation (iii)

Fig. 5 shows the minority carrier lifetime and the implied V_{oc} of wafers processed by SC-1,2 (group A) and SPM (group B) cleaning. It is clear that the average minority carrier lifetime (476.1 μ s and 478.8 μ s) or implied V_{oc} (702.4mV and 706.2mV) of both groups are close. However, the standard deviation of minority carrier lifetime (31.89) and implied V_{oc} (2.462) of SPM-disposed wafers are much smaller than that of SC-1,2-disposed wafers (71.61; 5.725), which also ascribes to the nonlinear and time-varying characteristic of SC-1,2 solutions. Thus SPM cleaning is a more stable and repeatable method compared with SC-1,2 cleaning in terms of minority carrier lifetime and implied V_{oc} .

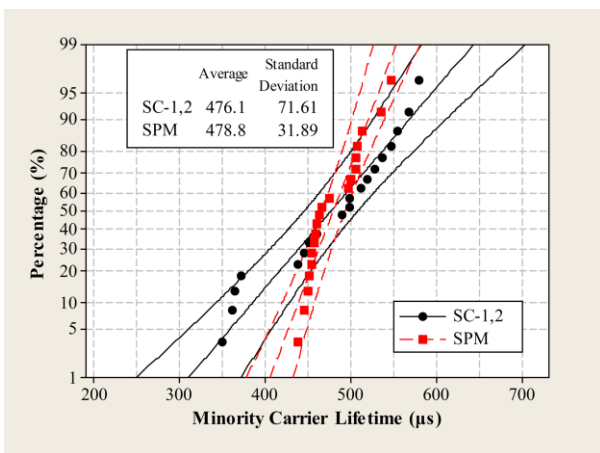


Fig. 5a. Wafers' minority carrier lifetime after SC-1,2 and SPM cleaning

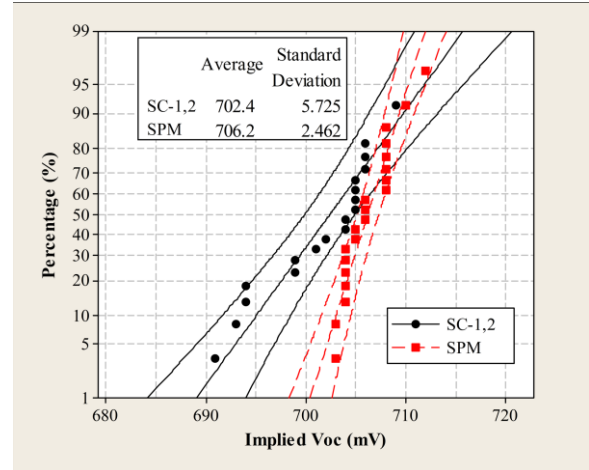


Fig. 5b. Wafers' implied V_{oc} after SC-1,2 and SPM cleaning

Moreover, SC-1,2 strategy contains 10 steps while SPM process only needs 4 steps, as shown in Fig. 1, which explains that SC-1,2 cleaning consumes more chemicals, energy and time. Meanwhile, SC-1,2 solutions, such as concentrated hydrochloric acid and aqueous ammonia, are tend to volatilize at room temperature and even more severely when be heated. These reasons lead to a much higher cost of SC-1,2 cleaning than that of SPM cleaning. Alternatively, were stability and repeatability to be taken into consideration, SC-1,2 cleaning is also inferior to SPM cleaning because of the nonlinear and time-varying property of SC-1,2 solutions. In general, SPM cleaning is more stable and cost-effective than SC-1,2 cleaning. Cells in this study can achieve a high V_{oc} with SPM cleaning.

3.2 Boron source for laser-doping: B_2H_6 or TMB

In order to simplify the fabrication process, PECVD was introduced to substitute for the dopant layer's spinning, baking and removing. PECVD-deposited SiO_2 layer (600nm) doped by B_2H_6 or TMB was selected as dopant layer. The ECV profiles of PVD Al after sintering and laser doped boron (B_4O , PBF1, B_2H_6 and TMB) are illustrated in Fig. 6.

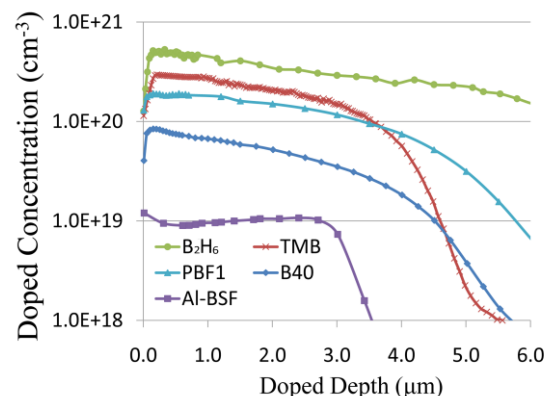


Fig. 6. Doping profiles of Al, B_4O , PBF1, B_2H_6 and TMB

The solid solubility of Al in silicon is $2 \times 10^{19} \text{cm}^{-3}$, while the solid solubility of boron in silicon is approximate 10^{21}cm^{-3} which is two orders bigger than that of Al. Thus the surface concentration of Al is $1.2 \times 10^{19} \text{cm}^{-3}$, whereas the surface concentration of B40, PBF1, B_2H_6 and TMB are $8.4 \times 10^{19} \text{cm}^{-3}$, $1.9 \times 10^{20} \text{cm}^{-3}$, $5.3 \times 10^{20} \text{cm}^{-3}$, $2.9 \times 10^{20} \text{cm}^{-3}$ respectively as depicted in Fig. 6. For B40 and PBF1 with boron source dissolved in organic solvents, the surface concentrations are smaller than that of B_2H_6 and TMB which is ascribed to the less boron content of liquid boron sources. In addition, it is important to point out that liquid boron sources (B40 and PBF1) contain many impurities. The subsequent low temperature (100°C - 150°C) baking after spinning cannot vaporize organics and other impurities thoroughly. In this case, the residual organics and impurities are pushed into the silicon bulk during laser doping which will cause a negative effect on electrical characteristics. Moreover, according to Fig. 6, B_2H_6 shows the highest concentration from surface to 6nm. Although TMB shows a relatively higher concentration compared with B40 and PBF1 from surface to 3.5nm, it drops sharply after 3.5nm. This consequence results from the boron content in both chemicals: 78.08% in B_2H_6 which is four times of 19.33% in TMB ($(\text{CH}_3)_3\text{B}$).

Considering the doping concentration, depth and purity, it is concluded that PECVD-deposited B_2H_6 source is the most appropriate boron source.

3.3 Boron source dopant layer $\text{SiO}_2(\text{B})$

Fig. 7 shows the doping profiles of boron with various thicknesses of $\text{SiO}_2(\text{B})$ (600nm, 400nm, 200nm and 100nm). The surface concentration decreases as the $\text{SiO}_2(\text{B})$ thickness drops: the surface boron concentration of 600nm $\text{SiO}_2(\text{B})$ is $6.5 \times 10^{20} \text{cm}^{-3}$; while 400nm, 200nm and 100nm correspond to $2.8 \times 10^{20} \text{cm}^{-3}$, $4.4 \times 10^{19} \text{cm}^{-3}$ and $1.9 \times 10^{19} \text{cm}^{-3}$, respectively. This is attributed to the higher boron volume that the thicker $\text{SiO}_2(\text{B})$ layer contains. It is

clear that the surface boron concentration of 100nm $\text{SiO}_2(\text{B})$ equals to that of Al ($1.2 \times 10^{19} \text{cm}^{-3}$) as shown in Fig. 6, which makes it meaningless to dope boron. Thus $\text{SiO}_2(\text{B})$ layer should be thicker in terms of doping concentration.

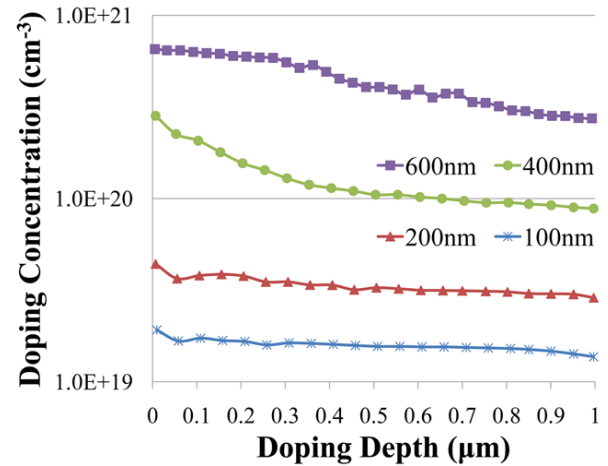


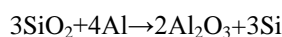
Fig. 7. Doping profiles of boron carried by SiO_2 with various thicknesses: 600nm, 400nm, 200nm, 100nm

However, the doping concentration is not the only factor that should be taken into account. Table 1 depicts the electrical characteristics of cells with various thicknesses of $\text{SiO}_2(\text{B})$ layer. Cells with 600nm $\text{SiO}_2(\text{B})$ demonstrates lowest average V_{oc} of 601.6mV, short-circuit currents density (J_{sc}) of 34.62mA/cm^2 , fill factors (FF) of 72.62% and efficiency (η) of 15.12%, while 100nm $\text{SiO}_2(\text{B})$ cells achieve the best performance with V_{oc} of 660.1mV, J_{sc} of 37.78mA/cm^2 , FF of 72.94% and η of 18.19%. As thickness rises, cells' performance shows adverse results.

Table 1. Electrical characteristics of cells with different thicknesses of $\text{SiO}_2(\text{B})$

Group	Duration(min)	D(nm)	V_{oc} (mV)	J_{sc} (mA/cm^2)	η (%)	FF(%)	R_s (mOhm)	R_{sh} (Ohm)
A	30	600	601.6	34.62	15.12	72.62	6.70	10.19
B	20	400	645.6	36.62	17.18	72.66	6.68	34.74
C	10	200	659.0	37.27	17.90	72.88	6.56	37.18
D	5	100	660.1	37.78	18.19	72.94	6.43	67.59

This may be caused by reaction between Al and SiO_2 during sintering process. The reaction is as follows [27]:



In this reaction process, Al replaces Si into Al_2O_3 , and consumes itself to reduce SiO_2 layer. Al layer which

detached by SiO_2 layer can serve as an effective rear reflector with a very high reflectivity of 97% [28]. However, after react with SiO_2 , part of Al transform into Al_2O_3 as one of the reaction products, with an inferior reflectivity compared with Al. The reflectivity of cells with 100nm, 200nm, 400nm and 600nm $\text{SiO}_2(\text{B})$ layer after sintering are shown in Fig. 8. The thicker the $\text{SiO}_2(\text{B})$

layer is, the lower the reflectivity at long wavelengths becomes. This is because thicker $\text{SiO}_2(\text{B})$ layer consumes more Al and more Al_2O_3 is formed. Moreover, Al is a good rear reflector, while Al_2O_3 is not. Thus the cells with 100nm $\text{SiO}_2(\text{B})$ layer demonstrate the highest reflectivity of 27% at 1200nm among the four groups. A low reflectivity at long wavelength corresponds to a low IQE, resulting in a low J_{sc} . However, 27% is still very low compared with the reflectivity of PERL cells (67% at 1200nm) in previous work [29].

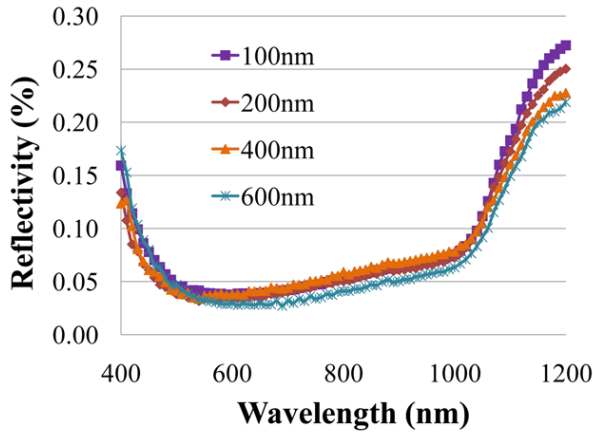


Fig. 8. Reflectivity of cells with 100nm, 200nm, 400nm and 600nm thick $\text{SiO}_2(\text{B})$ layer after sintering

In this experiment, $\text{SiO}_2(\text{B})$ layer was fabricated by 13.56 MHz RF PECVD. This direct PECVD induces surface damage because of direct ion bombardment. Moreover, since $\text{SiO}_2/\text{SiN}_x$ passivation layers were prepared via microwave remote PECVD, the stacks are relatively looser and would be damaged easily by ions generated during $\text{SiO}_2(\text{B})$ layer fabrication through RF PECVD. To manufacture a 100nm $\text{SiO}_2(\text{B})$ layer, five minutes are needed. By contrast, $\text{SiO}_2/\text{SiN}_x$ stacks, coated on rear silicon, have to undergo thirty minutes' RF PECVD to form a 600nm $\text{SiO}_2(\text{B})$ layer, which is six times as long as the duration of forming a 100nm $\text{SiO}_2(\text{B})$ layer. Therefore, as $\text{SiO}_2(\text{B})$ layer grown thicker, more time is required, which means that $\text{SiO}_2/\text{SiN}_x$ stacks experience more ion bombardment. It is deduced that the passivation effect of $\text{SiO}_2/\text{SiN}_x$ stacks would be sharply decreased as the ion bombardment duration increases. This deduction can be proved by V_{oc} of solar cells in Table 1: group A with 600nm $\text{SiO}_2(\text{B})$ shows the lowest V_{oc} of 601.6mV, while group D demonstrates the highest V_{oc} of 660.1mV.

Since the laser parameters and pattern of the four groups are the same and $\text{SiO}_2(\text{B})$ layer consumes part of laser energy to be ablated, the entire rear semi-metal contact area of thinner $\text{SiO}_2(\text{B})$ layer would be larger than that of thicker $\text{SiO}_2(\text{B})$ layer, as shown in Fig. 9. In this case, lateral resistance (one part of series resistance- R_s) of group D is the smallest, which results in a lowest series resistance as shown in Table 1.



Fig. 9a. Laser scanning microscope images of cells with 400nm $\text{SiO}_2(\text{B})$ after laser doping

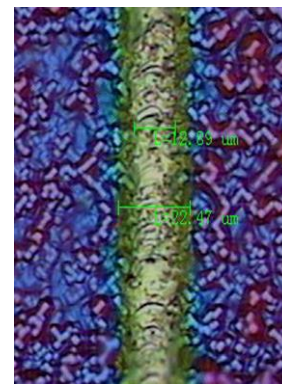


Fig. 9b. Laser scanning microscope images of cells with 200nm $\text{SiO}_2(\text{B})$ after laser doping



Fig. 9c. Laser scanning microscope images of cells with 100nm $\text{SiO}_2(\text{B})$ after laser doping

Besides, laser doping depends on thermal diffusion. Although thicker $\text{SiO}_2(\text{B})$ layer may not be ablated thoroughly, the boron atoms would diffuse into the silicon beneath the $\text{SiO}_2(\text{B})$ layer on where the laser irradiates, which results in a high doping concentration in silicon as shown in Fig. 7. However, the residual $\text{SiO}_2(\text{B})$ still exists on the laser path, as shown in Fig. 10. When Al is sputtered and sintered, $\text{Si}(\text{B})/\text{SiO}_2(\text{B})/\text{Al}$ structure is formed instead of $\text{Si}(\text{B})/\text{Al}$ structure. As a result, Schottky contact is formed as a substitute for ohmic contact.

Consequently, cells' total electrical characteristics, including V_{oc} , J_{sc} , R_s , shunt resistance (R_{sh}), FF and η , show a declining trend as $SiO_2(B)$ layer becomes thicker as demonstrated in Table 1.

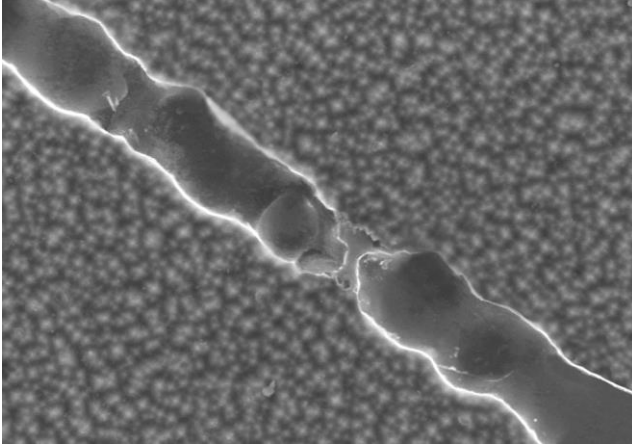


Fig. 10. SEM image of cell with 600nm $SiO_2(B)$ after laser doping

Additionally, no matter what the thickness of $SiO_2(B)$ layer is, the efficiency with the highest group being 18.19% is very low. The reason is that Al is seriously consumed by $SiO_2(B)$ and Al_2O_3 with low reflectivity in long wavelengths is formed. Furthermore, Al reduces the $SiO_2(B)$ layer and then localized pinholes are formed through the $SiO_2(B)$ layer [30]. Al contacts the Si surface

firstly through pinholes in $SiO_2(B)$ layer and then SiN_x layer. Besides, $SiO_2/SiN_x/SiO_2(B)$ stacks contain positive charges, which forms inversion layer at rear side. This "spiking" phenomenon has been known to cause shunting in MIS solar cells [31].

3.4 Boron dopant layer $SiN_x(B)$

Compared with SiO_2 , SiN_x is more stable when fired with Al back electrode. SiO_2 passivation layer cannot prevent Al-Si contact formation in places without laser holes, while SiN_x layer can [32]. Thus $SiN_x(B)$ is studied.

SiN_x thin film of very low reflectivity is often utilized as passivation and anti-reflection coating (ARC) layer on the front side [33]. However, SiN_x film on the rear side, acting as a reflector, should have very high reflectivity. Since reflectivity of a layer can be controlled through its refractive index (n) and thickness, the thickness of $SiN_x(B)$ is fixed at 100nm, and only the refractive index is varied. SiN_x dielectric layer shows a high passivation quality when refractive index is above 1.95 [34-35]. Therefore, $SiN_x(B)$ layers with 2.1 and 2.3 refractive index are investigated.

Electrical properties of cells with $SiN_x(B)$ layer are shown in Table 2. The performance is enhanced compared with cells with $SiO_2(B)$ layer. Cells of group A ($n=2.1$) demonstrate superior average V_{oc} (659.6mV), R_s (5.28mOhm), R_{sh} (438Ohm), FF (76.54%) and η (19.10%). There is no obvious difference on J_{sc} between two groups (only 0.1mA/cm²).

Table 2. Electrical characteristics of cells with different refractive index of $SiN_x(B)$

Group	n	V_{oc} (mV)	J_{sc} (mA/cm ²)	η (%)	FF(%)	R_s (mOhm)	R_{sh} (Ohm)
A	2.1	659.6	37.8	19.10	76.54	5.28	438
B	2.3	654.6	37.9	18.66	75.22	5.66	380

Song et al. [32] reported that the larger the refractive index of the SiN_x layer becomes, the easier the Al would be fired through. $SiN_x(B)$ layer with higher refractive index (2.3) is looser, thus Al fire-through is more likely to occur. This Al "fire-through" is the same with the Al "spiking" discussed in section 3.3. Also since the $SiO_2/SiN_x/SiN_x(B)$ stacks are positively charged as $SiO_2/SiN_x/SiO_2(B)$ stacks, it forms inversion layer at rear side. When $SiO_2/SiN_x/SiN_x(B)$ stacks are fired through, shunting would be caused in MIS solar cells. The mechanism of "fire-through" is identical with "spiking". Shunting causes lower V_{oc} and R_{sh} of group B.

Moreover, $SiN_x(B)$ layer with higher refractive index (2.3) contains more silicon, since refractive index increases as the amount of Si increases [32]. Thus boron

content is lower in $SiN_x(B)$ layer of group B compared with that of group A. After laser doping, the boron surface concentration of groups A and B are $3.6 \times 10^{19} \text{cm}^{-3}$ and $2.0 \times 10^{19} \text{cm}^{-3}$ respectively. Cells of group A achieve a better ohmic contact between Al and silicon, resulting in a smaller contact resistance. Correspondingly R_s of group A is 0.38mOhm smaller than that of group B (Table 2). With a higher R_{sh} and a lower R_s , cells of group A achieve a better FF and hence η .

3.5 Boron dopant layer a-Si(B)

Although cells' performance gets promoted by using $SiN_x(B)$ layer as boron dopant layer, the efficiency (19.10%) is still not ideal. In order to avoid parasitic

shunting caused by positive-charge-induced inversion layers due to SiO₂ or SiN_x when passivating p-type rear surfaces, dopant layer without positive charges is required. PECVD deposited a-Si is one of the rear surface passivation layers that were investigated and used as SiO₂ and SiN_x [36]. Thus a-Si(B) is chosen to substitute SiO₂(B) or SiN_x(B).

Table 3 summarized electrical characteristics of cells

with a-Si(B) under different firing conditions. Without firing, cells of group A show the highest R_s (8.0mOhm) and the lowest R_{sh} (275.9Ohm), which leads to the lowest FF (72.1%). Nevertheless, cells of groups B and C (fired at 600°C) demonstrate inferior V_{oc} (652.2mV and 644.3mV) and J_{sc} (36.4mA/cm² and 35.2mA/cm²), but superior FF (74.1% and 73.4%) compared with group A (678.9mV, 38.5mA/cm² and 72.1%).

Table 3. Electrical characteristics of cells with a-Si(B) under different firing conditions

Group	Temperature(°C)	Speed(mm/min)	V _{oc} (mV)	J _{sc} (mA/cm ²)	η(%)	FF(%)	R _s (mOhm)	R _{sh} (Ohm)
A	non-firing	non-firing	678.9	38.5	18.8	72.1	8.0	275.9
B	600	6000	652.2	36.4	17.6	74.1	6.7	760.2
C	600	3300	644.3	35.2	16.6	73.4	6.9	750.9
D	400	5000	676.5	38.2	19.4	75.2	6.5	767.3
E	400	2500	676.7	38.4	19.7	75.8	6.4	802.0
F	400	1100	677.1	38.5	19.8	76.0	6.2	874.7

Normally, a-Si layers are deposited, annealed or fired with Al at temperatures below approximately 400°C to reduce the loss of passivation properties, which is caused by hydrogen driving out and crystallization of a-Si. But a-Si(B) layer in this paper acts as boron dopant layer instead of passivation layer. Thus this deterioration of V_{oc} and J_{sc} may ascribe to the pinholes formed by Al through a-Si(B) layer during 600°C firing as V_{oc}, J_{sc} and FF further decreases with firing duration becoming longer (shown in Table 3). Compared with group A, FF of groups B and C are improved as a result of enhancement of Ohmic contact between Al and silicon in laser-opened area after 600°C firing.

As depicted in Table 3, cells of groups D, E and F (fired at 400°C) show similar V_{oc} and J_{sc} with group A, which explains that 400°C firing does not destroy the SiO₂/SiN_x/a-Si(B) stack. Comparatively, FF experiences a growth from group D (75.2%) to group F (76.0%) with firing duration increasing, which are all higher than that of group A (72.1%). Decrease of R_s (from 6.5mOhm of group D to 6.2mOhm of group F) is the main reason for the rise of FF. Thus it is deduced that 400°C, 1100mm/min firing can enhance the Ohmic contact between Al and silicon and can maintain the V_{oc} and J_{sc} at a stable level as group A. Cells here achieve an average efficiency of 19.8%.

4. Conclusions

In this paper, two cleaning methods (SC-1,2 and SPM) before passivation were investigated on purpose of enhancing passivation effect. Boron sources and dopant layers fabricated by RF PECVD were studied and selected for rear doping.

(1) SC-1,2 and SPM are two proposed methods to

cleaning wafers' surface. Considering the stability of the solutions and its cleaning effect, SPM was chosen to be the cost-effective method.

(2) Four boron doping sources were investigated: spinning-on liquid boron sources (B40 and PBF1) and PECVD-deposited solid boron sources (B₂H₆ and TMB). PECVD-deposited solid B₂H₆ source with its outstanding doping concentration, depth and purity was selected as the most appropriate boron source. In this case, the fabrication of dopant layer and the passivation layer (SiN_x) can be integrated into one process in the future since they are both formed by PECVD.

(3) Three kinds of boron dopant layers deposited by 13.56MHz RF PECVD were discussed: SiO₂(B) layer, SiN_x(B) layer and a-Si(B) layer. 100nm a-Si(B) layer without positive charges is the most suitable boron dopant layer. Cells experienced 400°C, 1100mm/min firing can achieve an average efficiency of 19.8%.

Acknowledgments

The authors would like to thank Jiangsu Provincial Research Center of Light Industrial Optoelectronic Engineering and Technology and Yongfei Jiang and Qi Qiao of Suntech Co., Ltd for their support in experiments and discussion.

References

- [1] A. Wang, J. Zhao, M. A. Green, Appl. Phys. Lett. **57**, 602 (1990).
- [2] J. Zhao, A. Wang, M. A. Green, Prog. Photovoltaics **7**, 471 (1999).
- [3] A. Das, R. Kyungsun, A. Rohatgi, IEEE J. Photovolt. **1**, 146 (2011).

- [4] A. Richter, J. Benick, M. Hermle, *IEEE J. Photovolt.* **3**, 235 (2013).
- [5] B. Veith, F. Werner, D. Zielke, R. Brendel, J. Schmidt, *Energy Procedia* **8**, 307 (2011).
- [6] P. Saint-Cast, M. Hofmann, T. Dimitrova, D. Wagenmann, J. Rentsch, R. Preu, Proc. 24-th EU PVSEC, Hamburg, Germany, 2009, p. 1649.
- [7] J. Horzel, P. Choulat, E. Cornagliotti, T. Janssens, J. John, I. Kuzma-Filipek, V. Prajapati, Proc. 27-th EU PVSEC, Frankfurt, Germany, 2012, p. 1602.
- [8] F. Colville, *Technical papers in Photovoltaic International Magazine* (5th ed.), 2010, p. 1.
- [9] S. Murarka, H. Levinstein, R. Marcus, R. Wagner, *J. Appl. Phys.* **48**, 4001 (1977).
- [10] A. Cacciato, F. Duerinckx, K. Baert, M. Moors, T. Caremans, G. Leys, K. De Keersmaecker, J. Szlufcik, *Sol. Energ. Mat. Sol. C.* **113**, 153 (2013).
- [11] J. Fairfield, Silicon diodes made by laser irradiation, *Solid State Electron.* **11**, 1175 (1968).
- [12] G. Turner, D. Tarrant, G. Pollock, R. Pressley, R. Press, *Appl. Phys. Lett.* **39**, 967 (1981).
- [13] U. Besi-Vetrella, G. Arabito, V. Barbarossa, E. Salza, F. Artuso, M. Belardinelli, M. Grilli, L. Pirozzi, Proc. 2nd World Conference and Exhibition on Photovoltaic Solar Energy Conversion, Vienna, Austria, 1998, p. 1366.
- [14] R. Stuck, E. Fogarassy, J. Muller, M. Hodeau, A. Wattiaux, P. Siffert, *Appl. Phys. Lett.* **38**, 715 (1981).
- [15] E. Fogarassy, R. Stuck, J. Grob, P. Siffert, *J. Appl. Phys.* **52**, 1076 (1981).
- [16] S. Eisele, G. Bilger, M. Ametowobla, J. Kohler, J. Werner, Proc. PVSEC, Milan, Italy, 2007, p. 715.
- [17] Z. Hameiri, L. Mai, T. Puzzer, S. Wenham, *Sol. Energ. Mat. Sol. C.* **95**, 1085 (2011).
- [18] B. Hallam, C. Chan, A. Sugianto, S. Wenham, *Sol. Energ. Mat. Sol. C.* **113**, 124 (2013).
- [19] S. Eisele, T. Roder, J. Kohler, J. Werner, *Appl. Phys. Lett.* **95**, 133501 (2009).
- [20] L. Wenjia, W. Zhenjiao, H. Peiyu, L. Hongyan, Y. Jian, G. Ying, S. Zhengrong, L. Guohua, *Appl. Surf. Sci.* **311**, 344 (2014).
- [21] S. Gall, B. Paviet-Salomon, J. Lerat, T. Emerald, *Energy Procedia* **27**, 449 (2012).
- [22] S. Gall, R. Hida, B. Paviet-Salomon, S. Manuel, Proc. 26-th EU PVSEC, Hamburg, Germany, 2011, p. 1648.
- [23] B. Paviet-Salomon, S. Gall, A. Slaoui, *Mater. Sci. Eng. B* **178**, 580 (2013).
- [24] S. Gall, S. Manuel, J. Lerat, *Energy Procedia* **38**, 270 (2013).
- [25] D. Schonauer, S. Avanzino, U.S. Patent No.5662769A (1997).
- [26] K. Shuichi, N. Takeshi, N. Hiroki, S. Takako, M. Mitsuru, I. Katsuyoshi, *Transactions of the Society of Instrument and Control Engineers* **37**, 754 (2001).
- [27] X. Cheng, X. Wu, L. Zhang, T. Chen, *Key Eng. Mater.* **249**, 269 (2003).
- [28] Y. Bai, A. Barnett, J. Rand, D. Ford, *Prog. Photovoltaics* **7**, 353 (1999).
- [29] Z. Wang, P. Han, H. Lu, H. Qian, L. Chen, Q. Meng, N. Tang, F. Gao, Y. Jiang, J. Wu, W. Wu, H. Zhu, J. Ji, Z. Shi, A. Sugianto, L. Mai, B. Hallam, S. Wenham, *Prog. Photovoltaics* **20**, 260 (2012).
- [30] A. Ho, S. Wenham, *Sol. Energ. Mat. Sol. C.* **91**, 1234 (2007).
- [31] R. Godfrey, M. Green, *Appl. Phys. Lett.* **34**, 860 (1979).
- [32] J. Song, S. Park, S. Kwon, S. Kim, H. Kim, S. Tark, S. Yoon, D. Kim, *Curr. Appl. Phys.* **12**, 313 (2012).
- [33] J.-F. Lelievre, E. Fourmond, A. Kaminski, O. Palais, D. Ballutaud, M. Lemiti, *Sol. Energ. Mat. Sol. C.* **93**, 1281 (2009).
- [34] T. Lauinger, J. Moschner, A. Aberle, R. Hezel, *J. Vac. Sci. Technol. A* **16**, 530 (1998).
- [35] D. Wright, E. Marstein, A. Rognmo, A. Holt, *Sol. Energ. Mat. Sol. C.* **92**, 1091 (2008).
- [36] H. Li, S. Wenham, Z. Shi, *Sol. Energ. Mat. Sol. C.* **117**, 41 (2013).

*Corresponding author: guohua_li55@yahoo.com